nature structural & molecular biology

Insights into voltage-gated calcium channel regulation from the structure of the $Ca_V1.2$ IQ domain–Ca^{2+}/calmodulin complex

Filip Van Petegem, Franck C Chatelain & Daniel L Minor, Jr

Changes in activity-dependent calcium flux through voltage-gated calcium channels (Ca_Vs) drive two self-regulatory calcium-dependent feedback processes that require interaction between Ca^{2+}/calmodulin (Ca^{2+}/CaM) and a Ca_V channel consensus isoleucine-glutamine (IQ) motif: calcium-dependent inactivation (CDI) and calcium-dependent facilitation (CDF). Here, we report the high-resolution structure of the Ca^{2+}/CaM–$Ca_V1.2$ IQ domain complex. The IQ domain engages hydrophobic pockets in the N-terminal and C-terminal Ca^{2+}/CaM lobes through sets of conserved 'aromatic anchors.' Ca^{2+}/N lobe adopts two conformations that suggest inherent conformational plasticity at the Ca^{2+}/N lobe–IQ domain interface. Titration calorimetry experiments reveal competition between the lobes for IQ domain sites. Electrophysiological examination of Ca^{2+}/N lobe aromatic anchors uncovers their role in $Ca_V1.2$ CDF. Together, our data suggest that Ca_V subtype differences in CDI and CDF are tuned by changes in IQ domain anchoring positions and establish a framework for understanding CaM lobe–specific regulation of Ca_Vs.

Voltage-gated calcium channels are the ion channels that define excitable cells[1]. These channels control cellular calcium entry in response to changes in membrane potential and are pivotal in the generation of cardiac action potentials, excitation-contraction coupling, hormone and neurotransmitter release and activity-dependent transcription initiation[1,2]. Ca_Vs are multisubunit complexes composed of three essential channel subunits[2], $Ca_V\alpha_1$, $Ca_V\beta$ and $Ca_V\alpha_2\delta$, plus the ubiquitous intracellular calcium sensor calmodulin (CaM)[3]. An additional subunit, $Ca_V\gamma$, is associated with skeletal muscle channels, but its general importance in other tissues is unsettled[4].

The $Ca_V\alpha_1$ subunits are single polypeptide chains of ~1,800–2,200 residues in which the ion-conducting pore is formed from four homologous repeats that each bear six transmembrane segments[2]. There are three Ca_V subfamilies, which have diverse physiological and pharmacological properties that depend largely on the $Ca_V\alpha_1$-subunit: Ca_V 1.*x* (L-type), Ca_V2.*x* (2.1, P/Q-type; 2.2, N-type; 2.3, R-type) and Ca_V3.*x* (T-type)[1]. Large interdomain intracellular loops bridge the four transmembrane repeats of the $Ca_V\alpha_1$ subunit and serve as docking sites for auxiliary subunits and regulatory molecules that control channel activity and connect Ca_V channels to larger macromolecular complexes and cellular signaling pathways[5,6].

Calcium influx is a potent activator of intracellular signaling pathways but is toxic in excess[1,7]. Because Ca_Vs are major sources of calcium influx, Ca_V activity is strongly controlled by both self-regulatory and extrinsic mechanisms that tune channel action in response to electrical excitation, neurotransmitter stimulation and hormonal cues[1,2,8]. This intense regulation uses multiple mechanisms and classes of intracellular signaling molecules. The bi-lobed calcium sensor CaM has a preeminent role in the intrinsic mechanisms of Ca_V calcium-dependent regulation[9–15]. Activity-dependent changes in intracellular calcium levels from flux through Ca_V channel pores drive two self-regulatory calcium-dependent feedback mechanisms that limit or enhance calcium entry through the channel: CDI and CDF[8]. Both require the interaction of Ca^{2+}/CaM with a consensus IQ motif in the $Ca_V\alpha_1$ C-terminal cytoplasmic tail[9,11–16].

Multiple lines of evidence suggest that CaM is constitutively tethered to the channel to detect calcium in the vicinity of the channel pore[12,17,18] and to permit calcium ions to exert control over their own entry through Ca_Vs. The nature of the tethering site remains unclear. It may comprise a region immediately adjacent to the IQ domain on the N-terminal side, termed the Pre-IQ region[17,19,20], or a composite of the Pre-IQ and IQ domain[18,20].

The IQ domain is believed to be the site of action of Ca^{2+}/CaM. Numerous studies show that Ca^{2+}/CaM binds IQ peptides from different Ca_V channels *in vitro*[9,11–14,17,20–22] and that IQ domain mutations in full-length channels can eliminate CDI[9,13–15,23] and CDF[9,14].

Although CDI and CDF are well documented, the details are complex, differ among channel subtypes and have not been readily predictable given the primary-sequence similarities among the Ca_V CaM-binding domains. Elegant experiments have demonstrated that CDI and CDF are controlled independently by the abilities of the

Cardiovascular Research Institute, Department of Biochemistry and Biophysics and Department of Cellular and Molecular Pharmacology, California Institute for Quantitative Biomedical Research, University of California, San Francisco, 1700 4th St., Box 2532, San Francisco, California 94143-2532, USA. Correspondence should be addressed to D.L.M. (daniel.minor@ucsf.edu).

Received 4 October; accepted 26 October; published online 20 November 2005; doi:10.1038/nsmb1027

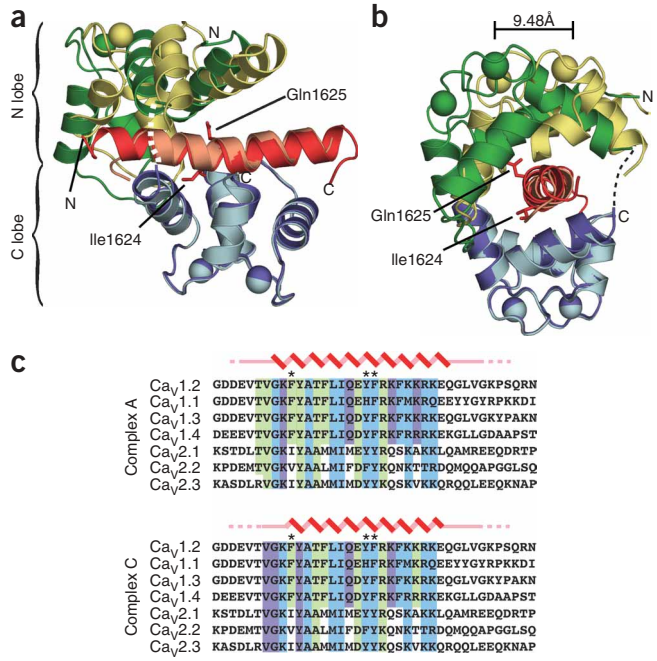

Figure 1 Structure of the Ca^{2+}/CaM–$Ca_V1.2$ IQ domain complex. (**a**) Ribbon diagram of the complex. Green, CaM Ca^{2+}/N lobe; blue, Ca^{2+}/C lobe; red, IQ domain, with residues Ile1624 and Q1625 from complex A in stick representation; darker shades, complex A; lighter shades, complex C. The complexes were superposed using the Ca^{2+}/C lobes and IQ domains. Labels indicate termini of components in complex A. Dashed lines indicate regions absent from the structures. (**b**) 90° rotation of **a**. The shift in Ca^{2+}/N lobe Ca^{2+} position in EF-hand 2 is indicated. (**c**) Sequence alignment of IQ regions from each Ca_V1 and Ca_V2 isoform. Zigzag, α-helical regions; straight line, nonhelical residues; dashed lines, residues present in the crystallized construct but absent from the electron density. Residues contacting CaM (≤4 Å) for conformation A and conformation C are highlighted as follows: green, contacts to Ca^{2+}/N lobe; cyan, Ca^{2+}/C lobe; purple, Ca^{2+}/N lobe and Ca^{2+}/C lobe. Asterisks indicate principal aromatic anchor positions. Sequences are human $Ca_V1.2$ 1609–1647, human $Ca_V1.1$ 1514–1552, rat $Ca_V1.3$ 1641–1679, human $Ca_V1.4$ 1563–1602, human $Ca_V2.1$ 1947–1985, human $Ca_V2.2$ 1845–1883 and rat $Ca_V2.3$ 1811–1850.

N-terminal and C-terminal CaM lobes (the N lobe and C lobe) to bind calcium[9,10,12,16,23]. CDI is present in both L-type ($Ca_V1.2$) and non–L-type ($Ca_V2.1$, $Ca_V2.2$ and $Ca_V2.3$) channels but arises from the action of opposite CaM lobes in these two cases[9,23]. In the L-type channel $Ca_V1.2$, CDI is governed by the binding of calcium ions to the C lobe[12], whereas in non–L-type channels (Ca_V2s), CDI is triggered by the binding of calcium ions to the N lobe[9,11,23]. In the non–L-type channel $Ca_V2.1$, CDF arises from interactions between calcium ions and the C lobe. Despite the fact that the C lobe–mediated processes elicit different channel behaviors in different channel subtypes, CDI in L-type and CDF in non–L-type channels, both C lobe processes share insensitivity to the fast calcium chelator BAPTA[23]. This shared resistance suggests that in both cases the C lobe captures calcium that is local to the channel pore[23]. In contrast, Ca_V2 N lobe–mediated CDF is sensitive to the slow calcium chelator EGTA, suggesting that it detects global changes in calcium concentration[9,23]. These lobe-specific calcium sensitivities have been suggested to provide mechanisms for Ca_Vs to sense, decode and distinguish local calcium changes due to calcium permeation through the channel from global calcium changes due to aggregate cellular signals[9,23].

To delineate the ways in which CDI and CDF arise, we set out to determine the molecular basis for Ca^{2+}/CaM interactions. Here, we report the high-resolution crystal structure of the human Ca^{2+}/CaM–$Ca_V1.2$ IQ domain complex. By using the structural data to inform functional experiments, we uncover an unexpected competition between the Ca^{2+}/CaM lobes for a common site on the IQ domain and demonstrate a previously unknown role for the Ca^{2+}/N lobe anchors in $Ca_V1.2$ CDF. This structure provides the first insight into the molecular machinery that underlies Ca^{2+}/CaM regulation of Ca_Vs.

RESULTS

Structure of the Ca^{2+}/CaM–$Ca_V1.2$ IQ domain complex

We solved the crystal structure of the Ca^{2+}/CaM–$Ca_V1.2$ IQ domain complex at 2.00-Å resolution using a three-wavelength MAD experiment on a selenomethionine (SeMet)-substituted protein crystal. The asymmetric unit contains three independent 1:1 Ca^{2+}/CaM–IQ domain complexes (complexes A, B and C) that have two principal conformations, represented by complexes A and C (**Fig. 1a**,**b**). Complex B is similar to complex A but has poorly defined density for the C-terminal half of the IQ domain (**Supplementary Fig. 1** online).

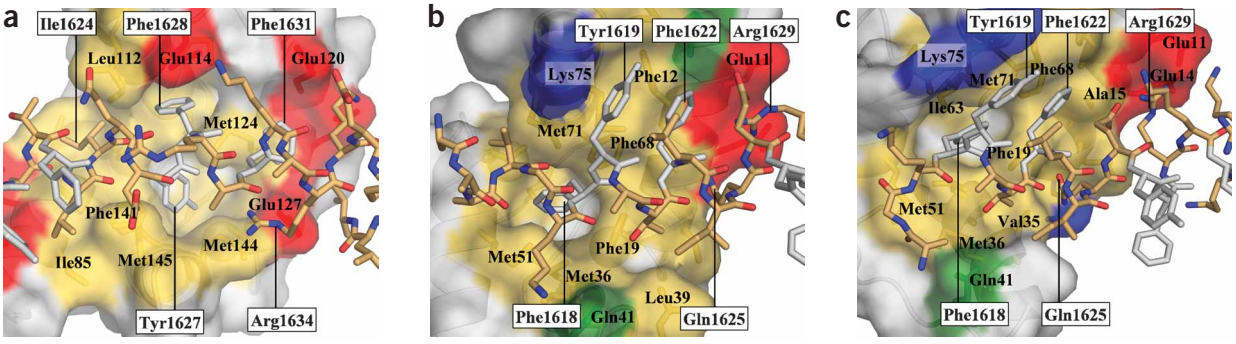

Figure 2 Lobe-specific Ca^{2+}/CaM–$Ca_V1.2$ IQ domain interactions. (**a**) Ca^{2+}/CaM C lobe from complex A bound to the IQ domain. Buried surface area = 1,819 $Å^2$ (965 $Å^2$ hydrophobic). (**b**) Ca^{2+}/CaM N lobe from complex A bound to the IQ domain. Buried surface area = 1,450 $Å^2$ (743 $Å^2$ hydrophobic). (**c**) Ca^{2+}/CaM N lobe from complex C bound to the IQ domain. Buried surface area = 1,491 $Å^2$ (500 $Å^2$ hydrophobic). IQ domain is shown in stick representation with aromatic anchor residues in white. CaM lobes are shown in surface representation with residues that contribute hydrophobic (yellow), negatively charged (red), positively charged (blue) and polar (green) side chain contacts (≤4 Å) to the IQ domain indicated. Select residues are labeled to orient the reader. IQ domain residue labels are boxed.

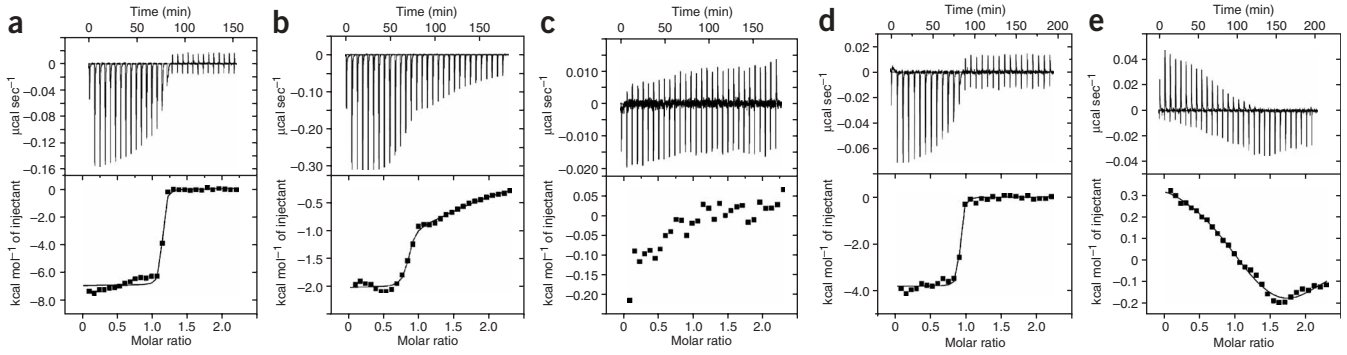

Figure 3 ITC characterization of Ca^{2+}/CaM–$Ca_V1.2$ IQ domain interactions. (**a**) 70 μM IQ domain into 7 μM Ca^{2+}/C lobe. (**b**) 500 μM Ca^{2+}/N lobe into 50 μM IQ domain. (**c**) 200 μM Ca^{2+}/N lobe into a solution of 20 μM IQ domain and 37 μM C lobe. (**d**) 60 μM IQ domain F1628A mutant into 6 μM Ca^{2+}/C lobe. (**e**) 500 μM Ca^{2+}/N lobe into a solution of 5 μM IQ domain F1628A mutant. Isotherms are fit to a single binding site model for **a** and **d** and a double binding site model for **b** and **e**. Panels show addition of 10 μl aliquots of titrant into the target solution (top) and binding isotherms (bottom).

Thus, our analysis focuses on the well-defined structures of complexes A and C. Both are compact structures in which Ca^{2+}/CaM embraces the largely α-helical IQ domain in a parallel orientation (**Fig. 1a**,**b**) through extensive interactions that involve twenty-two (complex A) or twenty-one (complex C) contiguous residues in the IQ domain, and both bury ~3,100 Å^2 total surface area of which roughly 1,650 Å^2 is hydrophobic (**Fig. 1c**). The observed parallel orientation in which Ca^{2+}/N lobe binds the N-terminal portion of the target helix and Ca^{2+}/C lobe binds the C-terminal portion is unusual and known in only one other Ca^{2+}/CaM peptide structure, the Ca^{2+}/CaM-dependent kinase peptide complex[24,25]. A high density of positively charged side chains project from the $Ca_V1.2$ IQ helix near the C terminus and make electrostatic interactions with negatively charged residues that ring the Ca^{2+}/CaM exit tunnel (**Fig. 2**). These interactions are consistent with the proposal that the distribution of positive charges on Ca^{2+}/CaM-binding peptides is an important determinant of binding orientation[24].

The Ca^{2+}/C lobes of complexes A and C are nearly identical (r.m.s. deviation for Cα atoms is 0.475) and are anchored similarly to the IQ domain helix (**Figs. 1** and **2**). The Ca^{2+}/N lobes are also similar (r.m.s. deviation for Cα atoms is 0.97) and have only small changes in the positions of side chains involved in direct contacts with the IQ peptide (**Supplementary Fig. 2** online). Superposition of Ca^{2+}/C lobes and IQ helices shows that the Ca^{2+}/N lobe adopts two distinct binding modes (**Fig. 1a**,**b**). In complex A, the Ca^{2+}/N lobe is positioned further along the N-terminal end of the IQ domain, whereas in complex C, the Ca^{2+}/N lobe is tilted and shifted toward the C-terminal end of the IQ domain, leading to a more compact conformation. The conformational differences cause relative displacements in the positions of the two Ca^{2+} ions in the Ca^{2+}/N lobe EF-hands of ~8.6 Å and ~9.5 Å and increase the bend present in both IQ domain helices at Ile1624 by ~10° in complex C.

Aromatic anchors mediate IQ domain–Ca^{2+}/CaM contacts

The $Ca_V1.2$ IQ helix engages Ca^{2+}/CaM through a set of 'aromatic anchor' residues. The C-terminal portion of the IQ helix displays three aromatic anchors (Tyr1627, Phe1628 and Phe1631) that bind hydrophobic Ca^{2+}/C lobe pockets. Two anchors (Tyr1627 and Phe1628) are deeply buried (**Fig. 2a**). The N-terminal part of the IQ helix presents three aromatic residues (Phe1618, Tyr1619 and Phe1622) that make hydrophobic interactions with the Ca^{2+}/N lobe; these residues reside on the opposite helical face from the C-terminal anchors. Phe1618 makes the most extensive contacts and binds a deep hydrophobic pocket (**Fig. 2b**,**c**). Despite the alternative positions of the Ca^{2+}/N lobe, Phe1618 remains buried in the same Ca^{2+}/N lobe hydrophobic pocket in both complexes by adopting different side chain rotamers (**Fig. 2b**,**c** and **Supplementary Fig. 2**).

Ca^{2+}/CaM interactions with IQ domain consensus residues

IQ domains are defined by the consensus sequence (I/L/V) QXXXRXXXX(R/K) (where X is any residue)[26,27]. The Ca^{2+}/CaM–$Ca_V1.2$ structure reveals the ways in which the hallmark residues of the IQ domain interact with the Ca^{2+}/CaM lobes. The Ile1624 side chain

Table 1 Thermodynamic parameters for $Ca_V1.2$ IQ domain–Ca^{2+}/CaM lobe interactions

	WT–Ca^{2+}/C lobe	WT–Ca^{2+}/N lobe	F1628A–Ca^{2+}/C lobe	F1628A–Ca^{2+}/N lobe
N_1	0.98 ± 0.18	0.85 ± 0.05	0.92 ± 0.04	0.96 ± 0.13
K_{d1} (nM)	2.63 ± 0.07	57.6 ± 35.5	2.59 ± 0.24	1,003 ± 567
ΔH_1 (kcal mol^{-1})	–6.77 ± 0.21	–1.91 ± 0.14	–3.69 ± 0.17	0.45 ± 0.02
ΔS_1 (cal mol^{-1} K^{-1})	15.75 ± 0.78	26.70 ± 0.85	26.45 ± 0.78	29.20 ± 1.13
ΔG_1 (kcal mol^{-1})	–11.31 ± 0.01	–9.60 ± 0.38	–11.31 ± 0.06	–7.96 ± 0.35
N_2		1.04 ± 0.0		1.0 ± 0.0
K_{d2} (nM)		19,190 ± 3,600		9,812 ± 8,220
ΔH_2 (kcal mol^{-1})		–1.42 ± 0.13		–0.67 ± 0.22
ΔS_2 (cal mol^{-1} K^{-1})		16.60 ± 0.84		21.00 ± 2.69
ΔG_2 (kcal mol^{-1})		–6.20 ± 0.11		–6.71 ± 0.55

Thermodynamic parameters of Ca^{2+}/C lobe and Ca^{2+}/N lobe binding to wild-type (WT) and F1628A $Ca_V1.2$ IQ domain at pH 7.4 in the presence of 1 mM $CaCl_2$. Each value corresponds to the mean of two separate experiments with different batches of both components (± s.d.).

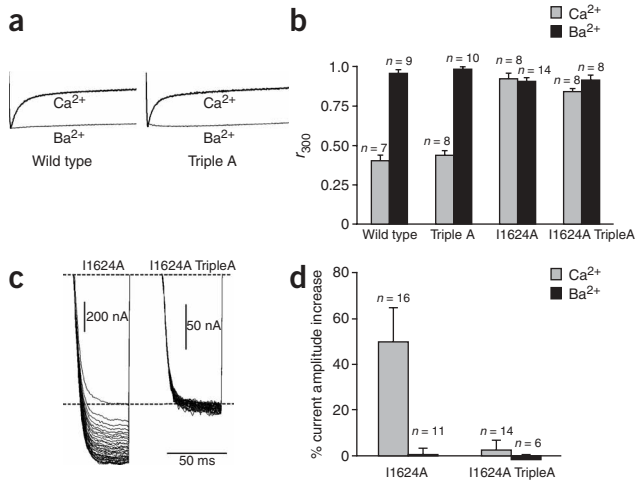

Figure 4 Lobe-specific interactions affect CDI and CDF. (**a**) Voltage-activated Ba^{2+} and Ca^{2+} currents from wild-type (WT) and TripleA channels during a 600-ms depolarizing step from –90 mV to +20 mV. Traces are normalized to the peak current to facilitate comparison. Tail currents are not shown. (**b**) r_{300} values (current fraction 300 ms after depolarization) in Ba^{2+} (black) and Ca^{2+} (grey). Error bars show s.d. (**c**) I1624A and I1624A TripleA Ca^{2+} currents in a 3-Hz 40-pulse train (50-ms steps to +20-mV from –90-mV holding potential). The first pulse currents are scaled to the same level for comparison. (**d**) Relative current increase between last and first pulses for I1624A and I1624A TripleA. Error bars show s.d.

is completely buried (solvent-exposed area = 0.7 Å^2) and contacts the hydrophobic surface of the C lobe (**Fig. 2a** and **Supplementary Figs. 2** and **3** online). The Gln1625 side chain has many contacts to the Ca^{2+}/N lobe. This residue also makes side chain and main chain water-mediated hydrogen bonds to the Ca^{2+}/C lobe (**Supplementary Figs. 2** and **3**). The central arginine, Arg1629, and terminal basic residue, Arg1634, form salt bridges with Glu11 and Glu14 of the Ca^{2+}/N lobe (**Supplementary Figs. 2** and **3**) and Glu127 of the Ca^{2+}/C lobe (**Supplementary Fig. 3**), respectively. Thus, all IQ hallmark residues seem important for IQ domain–Ca^{2+}/CaM interactions. These residues, together with the aromatic anchors and other positions throughout the IQ domain, establish the extensive network of contacts in the complex (**Supplementary Fig. 3**).

Isothermal titration calorimetry

We used isothermal titration calorimetry (ITC) to gain insight into the thermodynamics of lobe-specific Ca^{2+}/CaM–IQ domain interactions (**Fig. 3**). Ca^{2+}/C lobe binds the IQ domain with 1:1 stoichiometry and a high affinity ($K_d = 2.63 \times 10^{-9}$ M) that is driven by favorable enthalpic and entropic contributions (**Fig. 3a** and **Table 1**). Similar favorable components drive Ca^{2+}/N lobe binding; however, the isotherms revealed that there are two different binding sites, a medium-affinity ($K_d = 5.76 \times 10^{-8}$ M) and low-affinity ($K_d = 1.92 \times 10^{-5}$ M) site (**Fig. 3b** and **Table 1**). Both Ca^{2+}/N lobe–IQ domain interactions are substantially weaker than the Ca^{2+}/C lobe–IQ domain interaction. Titration of Ca^{2+}/N lobe into a solution containing Ca^{2+}/C lobe–IQ domain complexes yielded no further binding energy (**Fig. 3c**). These data directly demonstrate that the high-affinity Ca^{2+}/C lobe–IQ domain interaction occludes both measurable Ca^{2+}/N lobe–binding sites.

To investigate further whether the Ca^{2+}/N lobe– and Ca^{2+}/C lobe–binding sites depend on interactions observed in the crystal structure, we examined the consequence of a mutation in the IQ domain's aromatic anchor for Ca^{2+}/C lobe, F1628A. The F1628A mutant binds Ca^{2+}/C lobe with an affinity that is identical to the wild-type domain ($K_d = 2.59 \times 10^{-9}$ M), but with a reduced enthalpy (**Fig. 3d** and **Table 1**). This type of enthalpy-entropy compensation is a common feature in protein-protein interactions[28] and reflects a loss of key interactions in the bound state that is compensated by increased disorder. In contrast, the F1628A mutation causes a substantial perturbation of Ca^{2+}/N lobe medium-affinity binding ($K_d = 1.003 \times 10^{-6}$ M for F1628A compared to $K_d = 5.76 \times 10^{-8}$ M for the wild-type domain) and causes an unfavorable binding enthalpy. These data directly demonstrate that the medium-affinity Ca^{2+}/N lobe–binding site requires interactions with residues that comprise the crystallographically observed Ca^{2+}/C lobe site.

N lobe anchors have a role in CDF

Although Ca^{2+}/C lobe has an established role in $Ca_V1.2$ CDI[12,16,17], no role has yet been defined for Ca^{2+}/N lobe. Therefore, we tested whether the crystallographically observed Ca^{2+}/N lobe interface has a role in channel function by using two-electrode voltage clamp to interrogate mutant channels that were heterologously expressed in *Xenopus laevis* oocytes. A triple mutant lacking the three aromatic anchors for Ca^{2+}/N lobe (F1618A Y1619A F1622A), 'TripleA,' showed no appreciable difference in $Ca_V1.2$ inactivation when either Ca^{2+} or Ba^{2+} was the charge carrier (**Fig. 4a**,**b**). Thus, Ca^{2+}/N lobe–aromatic anchor interactions do not seem important for $Ca_V1.2$ CDI. This result agrees with the observation that overexpression of the CaM mutant CaM_{12}, in which the N lobe EF-hands have diminished calcium binding, has little effect on CDI[12,16]. TripleA channels consistently gave lower current amplitudes compared to wild-type channels. Previous reports have suggested a role for the IQ domain in Ca_V trafficking[29]; our observation raises the possibility that aromatic anchors for Ca^{2+}/N lobe may be important in this process.

Because the aromatic anchors for Ca^{2+}/N lobe are not crucial for $Ca_V1.2$ CDI, we asked whether they might have a role in CDF. CDF is a prominent property of $Ca_V2.1$ channels[9,10,30]. Although CDF is not readily detectable in wild-type $Ca_V1.2$ channels, robust CDF is unmasked by the I1624A mutation[14,15]. The I1624A mutation in the TripleA background (I1624A TripleA) results in channels lacking both CDI (**Fig. 4b**) and CDF (**Fig. 4c**,**d**). Lowering expression of a I1624A-only mutant such that current magnitudes were equivalent to those of the I1624A TripleA mutant still produced clear CDF (data not shown). This result excludes the possibility that CDF loss in I1624A TripleA is a consequence of the lower current magnitudes. Together, these experiments suggest that the aromatic anchors for the Ca^{2+}/N lobe have a previously unappreciated role in $Ca_V1.2$ CDF.

DISCUSSION

Calcium ions are potent chemical effectors of many cellular processes[1,7]. The opening of Ca_Vs in response to changes in membrane potential is a major source of calcium influx[1] and thus couples two forms of biological signals, electrical and chemical. The Ca_V activity that drives this powerful signaling combination is subject to a variety of control mechanisms. A diverse set of proteins that includes auxiliary channel subunits, G-proteins, synaptic vesicle components, kinases, phosphatases and calcium sensors interact with and modify the behavior of the pore-forming subunit to limit or enhance calcium influx[1,2].

Two types of feedback regulation in which calcium ions affect their own entry through Ca_Vs and control local calcium levels have been intensively studied for more than two decades[8]. CDI, which limits

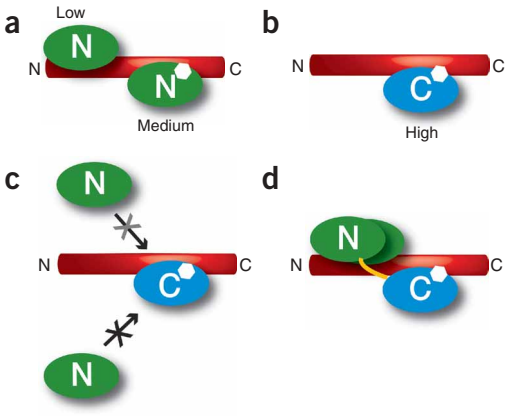

Figure 5 Schematic of Ca^{2+}/CaM lobe multiple binding modes on the $Ca_V1.2$ IQ domain. (**a**) Ca^{2+}/N lobe (green) has medium-affinity and low-affinity binding sites on the IQ domain. (**b**) Ca^{2+}/C lobe (blue) has a high-affinity binding site on the IQ domain. (**c**) Binding of Ca^{2+}/C lobe to the IQ domain blocks Ca^{2+}/N lobe access to the Ca^{2+}/N lobe medium-affinity site (black X) and reduces Ca^{2+}/N lobe binding to the Ca^{2+}/N lobe low-affinity site (grey X). (**d**) Representation of how Ca^{2+}/C lobe binding to the IQ domain tethers Ca^{2+}/N lobe near the Ca^{2+}/N lobe low-affinity site. Yellow line indicates the CaM interlobe linker. In all panels, the approximate position of aromatic anchor Phe1628, which is shared by the Ca^{2+}/N lobe medium-affinity site and the Ca^{2+}/C lobe high-affinity site, is indicated by the white hexagon.

calcium flux through Ca_Vs, and CDF, which enhances calcium flux through Ca_Vs, both result from interactions between calcium ions, a channel-resident CaM and the $Ca_V\alpha_1$ subunit's C-terminal cytoplasmic IQ domain[9,11–16,31]. Further dissection of the molecular origins of CDI and CDF has shown that each process arises from the binding of specific calcium-bound CaM lobes to the IQ domain[10,12–14]; however, the precise details have remained unknown.

IQ domains are protein segments that contain the 11-residue consensus sequence (I/L/V)QXXXRXXXX(R/K) and comprise a family of Ca^{2+}/CaM– and apo CaM–binding motifs found in diverse proteins including molecular motors, voltage-gated calcium channels, voltage-gated sodium channels and phosphatases[26,27]. The Ca^{2+}/CaM–IQ domain structure presented here offers the first high-resolution picture of the molecular details of a Ca^{2+}/CaM–IQ domain interaction. A previous work has proposed that Ile1624 is exposed in the Ca^{2+}/CaM–$Ca_V1.2$ complex to provide hydrophobic contacts to other parts of the channel-gating machinery[32]. Contrary to this prediction, the structure shows that Ile1624 is completely buried (solvent-exposed area = 0.7 Å^2) and contacts the hydrophobic surface of the C lobe (**Fig. 2a** and **Supplementary Figs. 2** and **3**). Other hallmark residues of the IQ domain engage in extensive hydrophobic and polar interactions with the CaM lobes that establish the importance of these residues for the Ca^{2+}/CaM–IQ domain interaction (**Fig. 1** and **Supplementary Figs. 2** and **3**).

The aromatic anchors that form the IQ domain's principal contacts to the Ca^{2+}/CaM lobes were not anticipated from prior studies. Comparison of the Ca_V IQ domain defined by the crystal structure with other IQ motifs reveals that many anchor positions are unique to Ca_Vs. Such an array of aromatic anchors, particularly the N-terminal anchors, is lacking in the C-terminal cytoplasmic IQ domains of the closely related family of voltage-gated sodium channels (Na_Vs)[33–35] (**Supplementary Fig. 4** online). This observation suggests that CaM binding to Ca_V and Na_V IQ domains and subsequent modulatory effects may be fundamentally different despite overall similarities in Na_V and Ca_V archictecture[1].

Examination of the Ca^{2+}/CaM–$Ca_V1.2$ IQ domain complexes shows interesting differences in the ways Ca^{2+}/N lobe and Ca^{2+}/C lobe interact with the IQ domain: the number of binding conformations differs, with two for Ca^{2+}/N lobe versus one for Ca^{2+}/C lobe; the number of deep anchor positions differs, with one for Ca^{2+}/N lobe (Phe1618) versus two for Ca^{2+}/C lobe (Tyr1627 and Phe1628); and the buried surface areas are not equivalent, as Ca^{2+}/C lobe buries more total and more hydrophobic surface than Ca^{2+}/N lobe (**Fig. 2**). These differences suggest that the Ca^{2+}/C lobe binds more tightly to the IQ domain. As it is not simple to infer directly the energetic importance of molecular interactions from structural data alone[36], we pursued experiments to determine whether these observed differences in modes of interaction have functional consequences.

We used ITC to probe the binding between the individual CaM lobes and the IQ domain. ITC experiments directly determine the thermodynamic parameters that underlie binding reactions and provide a degree of resolution for studying macromolecular interactions that is unmatched by other methods[37]. The experiments showed that the Ca^{2+}/C lobe binds the IQ domain with high affinity (K_d = 2.6 nM). To our surprise, we found multiple binding sites for the Ca^{2+}/N lobe on the IQ domain (**Fig. 5a**). The lack of appreciable Ca^{2+}/N lobe binding to the Ca^{2+}/C lobe–IQ domain complex (**Fig. 3c**), together with the large reduction in Ca^{2+}/N lobe binding affinity by the aromatic-anchor mutation F1628A (**Fig. 3e**), indicates that the medium-affinity Ca^{2+}/N lobe–binding site overlaps directly with the Ca^{2+}/C lobe–binding site (**Fig. 5**). The competition experiment (**Fig. 3c**) also showed that the binding of Ca^{2+}/C lobe to the IQ domain lowers the affinity of the second Ca^{2+}/N lobe–binding site to an undetectable level (K_d > 200 μM, given the concentrations used in the experiment[37]). The dominance of Ca^{2+}/C lobe in IQ domain binding energetics agrees with the eminent role of the Ca^{2+}/C lobe in CDI of L-type channels[12,16,17]. Given that the medium-affinity Ca^{2+}/N lobe site overlaps with the high-affinity Ca^{2+}/C lobe site and that Ca^{2+}/C lobe binding to its high-affinity site weakens the avidity of Ca^{2+}/N lobe for its low-affinity site, the thermodynamic data suggest that the crystallographically observed Ca^{2+}/N lobe interactions correspond to the Ca^{2+}/N lobe low-affinity site. These interactions arise from the high effective concentration[38] of the Ca^{2+}/N lobe relative to the peptide caused by Ca^{2+}/C lobe binding and the CaM interlobe linker (**Fig. 5d**).

As Ca^{2+}/C lobe binds tighter than Ca^{2+}/N lobe to the site that includes Phe1628, Ca^{2+}/N lobe is not expected to occupy this part of the IQ domain when both CaM lobes are loaded with calcium. However, Ca^{2+}/N lobe may occupy this position in channel functional states in which the N lobe is loaded with calcium but the C lobe is in the apo state. This property may be particularly relevant for Ca_V2s, where functional experiments have demonstrated that CaM mutants that have diminished C lobe calcium binding but preserve N lobe calcium binding maintain CDI[9,11,23].

Functional studies indicate lobe-specific tasks for CaM in Ca_V regulation[9,12,16,17,23]. The interactions that bring about lobe-specific regulation by CaM have remained obscure despite the investigation of an abundance of mutations to the IQ domain[13–15,17,18,32]. In the context of the structure, it is clear that most of the reported $Ca_V1.2$ mutants, many of which involve multiple residue changes, alter contacts to both lobes simultaneously and therefore cannot be used to decipher the roles of binding to each lobe individually. The exceptions are mutants having changes at two single positions that contact the Ca^{2+}/C lobe, Ile1624 and Phe1628 (refs. 14,15). Ile1624

mutations that perturb the residue's hydrophobicity and size disrupt CDI[15]. F1628A changes channel inactivation properties[15]. Together, these results indicate that the crystallographically defined IQ domain interface that contacts the Ca^{2+}/C lobe is important for channel inactivation.

Both CaM lobes have specific functional roles in modulation of Ca_V2 channels[9,11,23]. There is a clear role for the Ca^{2+}/C lobe in Ca_V1 CDI. Ca_V1s and Ca_V2s are highly homologous in the region that interacts with CaM to mediate CDF and CDI. Despite the similarity, no role has yet been reported for the N lobe in Ca_V1 modulation. We tested whether the Ca^{2+}/N lobe–anchoring residues observed in the Ca^{2+}/CaM–IQ domain structure had a functional role. Simultaneous mutation of all three aromatic anchors for the N lobe to alanine did not affect $Ca_V1.2$ CDI (**Fig. 4a**,**b**). In contrast, these same mutations in the background of the I1624A mutation, which unmasks $Ca_V1.2$ CDF, completely disrupted $Ca_V1.2$ CDF, demonstrating a clear role for this Ca^{2+}/N lobe interface in CDF (**Fig. 4c**,**d**). These experiments define a previously unknown role for the N lobe interface and suggest that the Ca^{2+}/N lobe conformations seen in the structure are important for CDF. Apo CaM can also bind the IQ domain[18,20]. It remains possible that the functional effects we observed have more complex origins that arise from interplay between Ca^{2+}/CaM– and apo CaM–IQ domain binding.

The dual binding mode of Ca^{2+}/N lobe observed in the structure suggests a level of conformational plasticity in Ca^{2+}/N lobe–channel interactions. Regions on the N-terminal side of the IQ domain bind Ca^{2+}/CaM *in vitro*[17,19–21,39], but with lower affinity than the IQ domain does[17,20]. Anchoring of the Ca^{2+}/C lobe to the IQ domain may permit Ca^{2+}/CaM to remain bound while other regions of the channel compete for Ca^{2+}/N lobe or the Ca^{2+}/N lobe aromatic anchors during various states of channel operation[17,39,40]. Alternatively, the observed conformational plasticity may provide a means for the complex to accommodate conformational changes that facilitate interactions with other channel domains while maintaining the Ca^{2+}/N lobe–IQ interaction.

Ca_V2s show lobe-specific Ca^{2+}/CaM modulation that seems inverted relative to $Ca_V1.2$ (refs. 9,11,23). Ca_V2 CDI relies on the Ca^{2+}/N lobe[9,11,23], whereas the prominent CDF of $Ca_V2.1$ originates with the Ca^{2+}/C lobe[9,11]. The ITC data show that the Ca^{2+}/N lobe–binding sites in the $Ca_V1.2$ IQ domain overlap with the Ca^{2+}/C lobe–binding site. It is notable that three aromatic anchors identified here, Phe1618, Phe1622 and Phe1631, including Ca^{2+}/N lobe aromatic anchor Phe1618, are conserved among Ca_V1s but not between Ca_V1s and Ca_V2s (**Fig. 1c**). Amino acid substitutions at these positions, together with changes at Gln1625 and Lys1633 (**Fig. 1c**), may tilt the Ca^{2+}/N lobe– and Ca^{2+}/C lobe–IQ domain affinity differences in favor of the Ca^{2+}/N lobe. Such changes, in concert with interactions to other parts of the channel, may underlie the fundamental differences in lobe-specific modulation between $Ca_V1.2$ and Ca_V2s in a way that exploits the prodigious adaptability of CaM to recognize varied targets[41].

The Ca^{2+}/CaM–$Ca_V1.2$ IQ domain structure presented here is the first high-resolution view of the components that transduce Ca^{2+}-dependent Ca_V regulation, and it provides a necessary molecular framework for detailed dissection of the transitions that drive the rich regulation of Ca_Vs by CaM.

METHODS

Purification. The IQ domain of human $Ca_v1.2$ ($Ca_V\alpha_1$c77) (residues 1611–1644), human CaM N lobe (residues 1–78) and human CaM C lobe (residues 79–148) were cloned into a modified pET28 vector (Novagen) denoted HMT[42] that contains, in sequence, a His_6-tag, maltose-binding protein and a cleavage site for the tobacco etch virus (TEV) protease. Full-length CaM was cloned into pEGST[43] without using any affinity tag. The F1628A mutation in the IQ domain was obtained using the QuikChange protocol (Stratagene).

All proteins were expressed in *Escherichia coli* BL21(DE3)pLysS grown in 2× YT media at 37 °C. Cells were lysed in 250 mM KCl, 10 mM K-HEPES (pH 7.4) and 1 mM $CaCl_2$ (buffer A) supplemented with 1 mM PMSF. The complex of CaM and IQ domain was obtained by coexpression and was purified on a Poros20MC column (Perseptive Biosystems), washed with buffer A and eluted with buffer A plus 500 mM imidazole (buffer B). After cleavage with His-tagged TEV protease[44] at room temperature for ~12 h and dialysis against 100 mM KCl, 10 mM Tris-HCl (pH 8.8) and 1 mM $CaCl_2$ (buffer C), the complex was purified on a Hiload HQ column (Amersham) in buffer C with a linear gradient to 30% buffer D (1 M KCl, 10 mM Tris-HCl (pH 8.8), 1 mM $CaCl_2$). Trace amounts of residual maltose-binding protein were removed by collecting the flow-through from an additional passage of the purified material over a

Table 2 Data collection, phasing and refinement statistics

	Native	SeMet		
Data collection				
Space group	$P2_1$	$P2_1$		
Cell dimensions				
a, *b*, *c* (Å)	84.73, 37.24, 86.86	82.55, 37.01, 87.55		
α, β, γ (°)	90, 97.77, 90	90, 98.10, 90		
		Peak	*Inflection*	*Remote*
Wavelength	1.116	0.97957	0.97972	1.01986
Resolution (Å)	30.0–2.0 (2.07–2.0)	30–2.5 (2.59–2.50)	30–2.8 (2.90–2.80)	30–2.4 (2.49–2.40)
R_{sym}	6.6 (33.1)	9.5 (42.8)	7.4 (40.1)	6.6 (34.3)
$I / \sigma I$	19.8 (2.2)	19.0 (2.5)	14.2 (2.1)	15.0 (1.7)
Completeness (%)	99.2 (98.3)	97.1 (99.4)	99.9 (100)	87.1 (89.6)
Redundancy	3.5	7.8	3.8	2.6
Refinement				
Resolution (Å)	30.0–2.0			
No. reflections	36,436			
R_{work} / R_{free}	20.23 / 25.47			
No. atoms				
Protein	3,845			
Ligand/ion	15			
Water	260			
B-factors				
Protein	31.50			
Ligand/ion	38.16			
Water	47.05			
R.m.s. deviations				
Bond lengths (Å)	0.016			
Bond angles (°)	1.363			

One native and one SeMet crystal were used for structure solution. Highest-resolution shell is shown in parentheses.

Poros20MC column in buffer A. Finally, the sample was dialyzed against 20 mM KCl, 10 mM K-HEPES (pH 7.4) and 1 mM $CaCl_2$.

SeMet-substituted complex was expressed in BL21(DE3)pLysS cells in M9 minimal medium containing 20% (w/v) glucose, with the methionine biosynthesis pathway inhibited[45]. Purification was as described above with all buffers supplemented with 5 mM methionine and 10 mM β-mercaptoethanol.

The first steps of purifying HMT–CaM N lobe and HMT–CaM C lobe fusions were similar to the CaM–IQ domain purification. After TEV cleavage, the material was dialyzed against buffer E (10 mM Tris-HCl (pH 8.8), 10 mM KCl, 1 mM $CaCl_2$) and purified on a Hiload HQ column with a gradient from 0 to 50% buffer F (1 M KCl, 10 mM Tris-HCl (pH 8.8), 1 mM $CaCl_2$). The proteins were purified further on a Poros20MC column in buffer A, and the concentrated flow-through was applied to a TSK2000 column (Tosoh Biosep) run in buffer A.

To obtain free IQ domain we purified the complex with CaM as described above and separated the two components on a preparative C18 HPLC column (Vydac) with a linear gradient from 35 to 50% acetonitrile in 0.1% (v/v) trifluoroacetic acid over 15 column volumes. The purity was verified by MALDI-TOF mass spectrometry.

Crystallization and structure determination. Complexes of native and SeMet-substituted CaM–IQ domain were crystallized by sitting or hanging drop vapor diffusion[46] at 20 °C by mixing equal volumes of protein (~10 mg ml^{-1}) and well solution containing 0.1 M Bis-Tris (pH 6.5) and 20–30% (w/v) PEG 3350. After transfer to Paratone oil (Hampton Research) and flash-freezing, diffraction data were collected at Beamline 8.3.1 (Advanced Light Source, Lawrence Berkeley National Laboratories) and processed using HKL2000 (ref. 47). A three-wavelength MAD experiment was performed on crystals of SeMet-substituted protein (**Table 2**). Twenty-five initial selenium positions were located using ShelxD[48]. Subsequent refinement, substructure completion and phasing were performed using SHARP[49] (**Supplementary Fig. 1**). After density modification the figure of merit was 0.852. An initial model was built using RESOLVE[50] and ARP/wARP[51], manually extended with XtalView[52] and refined against 2.00-Å native data using REFMAC5 (ref. 53). TLS parameters were used throughout the refinement. Side chains and full residues with missing electron densities were not modeled. The final model consists of three Ca^{2+}/CaM–IQ domain complexes in the asymmetric unit with 95.2% of the residues in the core region of the Ramachandran plot and none in disallowed regions. A Ni^{2+} ion is observed in all three complexes and most likely was introduced into the sample from the Ni^{2+} affinity column (Poros20MC). Its presence in the crystal was confirmed by a fluorescence wavelength scan. The Ni^{2+} binds at the C lobe outer surface distal from the IQ domain and is not expected to interfere with Ca^{2+}/CaM–IQ domain binding. Refinement data and statistics are shown in **Table 2**.

Isothermal titration calorimetry. Samples were concentrated and dialyzed twice against 5 mM KCl, 10 mM HEPES (pH 7.4) and 1mM $CaCl_2$. Higher salt concentrations reduced the solubility of the IQ domain. Samples were degassed for 5 min and titrations were performed on a VP-ITC calorimeter (MicroCal) at 15 °C. Data were processed with MicroCal Origin 7.0. For fitting of the F1628A N lobe data, the stoichiometry for the second binding site was set equal to 1. Because of the high titrant concentration required to measure weak interactions, and owing to limited solubility of the IQ domain, N lobe was titrated into peptide and not vice versa.

Protein concentrations were determined by absorbance[54], except for N lobe CaM (which has no aromatic residues), where the BCA method was used, using known concentrations of full-length CaM and CaM C lobe as references. Each ITC experiment was repeated with different batches of purified protein, yielding similar thermodynamic parameters and stoichiometry values. Control injections, consisting of titrating one component into buffer, were used to adjust the baseline of each experiment.

Electrophysiology. Constructs for electrophysiology consisted of human $Ca_V1.2$ (splice variant α_1c77) in pcDNA3.1(+)/hygro (Invitrogen), $Ca_V\beta_{2a}$ in pGEM (Promega) and rabbit $Ca_V\alpha_2\delta$ in pcDNA3 (Invitrogen). Mutants of the α_1c77 subunit were made using the QuikChange protocol (Stratagene). RNA transcripts were prepared using a T7 mMessage mMachine kit (Ambion). 50 nl of a complementary RNA mixture containing 30–100 nM $Ca_V1.2$ α_1c77, 33 nM $Ca_V\beta_{2a}$ and 33 nM $Ca_V\alpha_2\delta$ was microinjected into *Xenopus* oocytes, which were then kept at 18 °C in ND96 medium supplemented with penicillin and streptomycin. Recordings were performed 3–7 d after injection. Before recording, oocytes were injected with 25–50 nl 100 mM BAPTA to minimize contaminating Ca^{2+}-activated Cl^- current. During recordings, the oocytes were superfused using a Valvelink 16 (Automate Scientific) controller with either a Ba^{2+}-containing solution (40 mM $Ba(OH)_2$, 50 mM NaOH, 1 mM KOH, 0.4% (w/v) niflumic acid, 10 mM HEPES) or a Ca^{2+}-containing solution ($Ba(OH)_2$ replaced with $Ca(NO_3)_2$). Both solutions were adjusted to pH 7.4 using HNO_3. Two-electrode voltage-clamp experiments were performed using a GeneClamp 500B amplifier (Axon Instruments) controlled by a computer with a 1,200 MHz processor (Celeron, Gateway) using CLAMPEX 8.2.0.224 (Axon Instruments) and digitized at 1 kHz with a Digidata1332A (Axon Instruments). Electrodes were filled with 3 M KCl and had resistances of 0.1–1.5 MΩ. Leak currents were subtracted using a P/4 protocol. Ionic currents were analyzed with Clampfit 8.2 (Axon Instruments).

Accession codes. Protein Data Bank: Coordinates have been deposited with accession code 2BE6.

Note: Supplementary information is available on the Nature Structural & Molecular Biology website.

ACKNOWLEDGMENTS

We thank K. Brejc and D. Fass for comments on the manuscript; J. Holton at Beamline 8.3.1 at the Advanced Light Source for help with data collection; C.B. Klee (US National Institutes of Health, Bethesda, Maryland, USA) for the calmodulin clone; R.W. Tsien (Stanford University School of Medicine, Stanford, California, USA) and D.T. Yue (Johns Hopkins University School of Medicine, Baltimore, USA) for calcium channel clones; and members of the Minor laboratory for support at all stages of this work. This work was supported by awards to D.L.M. from the McKnight Foundation for Neuroscience, the Rita Allen Foundation, the Alfred P. Sloan Foundation and the US National Institutes of Health and to F.V.P. from the American Heart Association Western States Affiliate. D.L.M. is a McKnight Scholar in Neurosciences, an Alfred P. Sloan Research Fellow and a Rita Allen Foundation Scholar.

COMPETING INTERESTS STATEMENT

The authors declare that they have no competing financial interests.

Published online at http://www.nature.com/nsmb/
Reprints and permissions information is available online at http://npg.nature.com/reprintsandpermissions/

1. Hille, B. *Ion Channels of Excitable Membranes* (Sinauer Associates, Inc., Sunderland, Massachusetts, USA, 2001).
2. Catterall, W.A. Structure and regulation of voltage-gated Ca^{2+} channels. *Annu. Rev. Cell Dev. Biol.* **16**, 521–555 (2000).
3. Saimi, Y. & Kung, C. Calmodulin as an ion channel subunit. *Annu. Rev. Physiol.* **64**, 289–311 (2002).
4. Kang, M.G. & Campbell, K.P. Gamma subunit of voltage-activated calcium channels. *J. Biol. Chem.* **278**, 21315–21318 (2003).
5. Sheng, Z.H., Westenbroek, R.E. & Catterall, W.A. Physical link and functional coupling of presynaptic calcium channels and the synaptic vesicle docking/fusion machinery. *J. Bioenerg. Biomembr.* **30**, 335–345 (1998).
6. Walker, D. & De Waard, M. Subunit interaction sites in voltage-dependent Ca^{2+} channels: role in channel function. *Trends Neurosci.* **21**, 148–154 (1998).
7. Kandel, E.R., Schwartz, J.H. & Jessell, T.M. *Principles of Neural Science* (McGraw-Hill, New York, USA, 2000).
8. Budde, T., Meuth, S. & Pape, H.C. Calcium-dependent inactivation of neuronal calcium channels. *Nat. Rev. Neurosci.* **3**, 873–883 (2002).
9. DeMaria, C.D., Soong, T.W., Alseikhan, B.A., Alvania, R.S. & Yue, D.T. Calmodulin bifurcates the local Ca^{2+} signal that modulates P/Q-type Ca^{2+} channels. *Nature* **411**, 484–489 (2001).
10. Lee, A. *et al.* Ca^{2+}/calmodulin binds to and modulates P/Q-type calcium channels. *Nature* **399**, 155–159 (1999).
11. Lee, A., Zhou, H., Scheuer, T. & Catterall, W.A. Molecular determinants of Ca^{2+}/calmodulin-dependent regulation of Cav2.1 channels. *Proc. Natl. Acad. Sci. USA* **100**, 16059–16064 (2003).
12. Peterson, B.Z., DeMaria, C.D., Adelman, J.P. & Yue, D.T. Calmodulin is the Ca^{2+} sensor for Ca^{2+}-dependent inactivation of L-type calcium channels. *Neuron* **22**, 549–558 (1999).
13. Qin, N., Olcese, R., Bransby, M., Lin, T. & Birnbaumer, L. Ca^{2+}-induced inhibition of the cardiac Ca^{2+} channel depends on calmodulin. *Proc. Natl. Acad. Sci. USA* **96**, 2435–2438 (1999).

14. Zühlke, R.D., Pitt, G.S., Deisseroth, K., Tsien, R.W. & Reuter, H. Calmodulin supports both inactivation and facilitation of L-type calcium channels. *Nature* **399**, 159–162 (1999).
15. Zühlke, R.D., Pitt, G.S., Tsien, R.W. & Reuter, H. Ca^{2+}-sensitive inactivation and facilitation of L-type Ca^{2+} channels both depend on specific amino acid residues in a consensus calmodulin-binding motif in the (alpha)1C subunit. *J. Biol. Chem.* **275**, 21121–21129 (2000).
16. Alseikhan, B.A., DeMaria, C.D., Colecraft, H.M. & Yue, D.T. Engineered calmodulins reveal the unexpected eminence of Ca^{2+} channel inactivation in controlling heart excitation. *Proc. Natl. Acad. Sci. USA* **99**, 17185–17190 (2002).
17. Pitt, G.S. *et al.* Molecular basis of calmodulin tethering and Ca^{2+}-dependent inactivation of L-type Ca^{2+} channels. *J. Biol. Chem.* **276**, 30794–30802 (2001).
18. Erickson, M.G., Liang, H., Mori, M.X. & Yue, D.T. FRET two-hybrid mapping reveals function and location of L-type Ca^{2+} channel CaM preassociation. *Neuron* **39**, 97–107 (2003).
19. Romanin, C. *et al.* Ca(2+) sensors of L-type Ca(2+) channel. *FEBS Lett.* **487**, 301–306 (2000).
20. Tang, W. *et al.* Apocalmodulin and Ca^{2+} calmodulin-binding sites on the CaV1.2 channel. *Biophys. J.* **85**, 1538–1547 (2003).
21. Pate, P. *et al.* Determinants for calmodulin binding on voltage-dependent Ca^{2+} channels. *J. Biol. Chem.* **275**, 39786–39792 (2000).
22. Black, D.J. *et al.* Calmodulin interactions with IQ peptides from voltage-dependent calcium channels. *Am. J. Physiol. Cell Physiol.* **288**, C669–C676 (2005).
23. Liang, H. *et al.* Unified mechanisms of Ca(2+) regulation across the Ca(2+) channel family. *Neuron* **39**, 951–960 (2003).
24. Osawa, M. *et al.* A novel target recognition revealed by calmodulin in complex with Ca^{2+}-calmodulin-dependent kinase kinase. *Nat. Struct. Biol.* **6**, 819–824 (1999).
25. Kurokawa, H. *et al.* Target-induced conformational adaptation of calmodulin revealed by the crystal structure of a complex with nematode Ca(2+)/calmodulin-dependent kinase kinase peptide. *J. Mol. Biol.* **312**, 59–68 (2001).
26. Bahler, M. & Rhoads, A. Calmodulin signaling via the IQ motif. *FEBS Lett.* **513**, 107–113 (2002).
27. Jurado, L.A., Chockalingam, P.S. & Jarrett, H.W. Apocalmodulin. *Physiol. Rev.* **79**, 661–682 (1999).
28. Dunitz, J.D. Win some, lose some: enthalpy-entropy compensation in weak intermolecular interactions. *Chem. Biol.* **2**, 709–712 (1995).
29. Gao, T., Bunemann, M., Gerhardstein, B.L., Ma, H. & Hosey, M.M. Role of the C terminus of the alpha 1C (CaV1.2) subunit in membrane targeting of cardiac L-type calcium channels. *J. Biol. Chem.* **275**, 25436–25444 (2000).
30. Lee, A., Scheuer, T. & Catterall, W.A. Ca^{2+}/calmodulin-dependent facilitation and inactivation of P/Q-type Ca^{2+} channels. *J. Neurosci.* **20**, 6830–6838 (2000).
31. Zühlke, R.D. & Reuter, H. Ca^{2+}-sensitive inactivation of L-type Ca^{2+} channels depends on multiple cytoplasmic amino acid sequences of the alpha1C subunit. *Proc. Natl. Acad. Sci. USA* **95**, 3287–3294 (1998).
32. Kim, J., Ghosh, S., Nunziato, D.A. & Pitt, G.S. Identification of the components controlling inactivation of voltage-gated Ca^{2+} channels. *Neuron* **41**, 745–754 (2004).
33. Deschenes, I. *et al.* Isoform-specific modulation of voltage-gated Na(+) channels by calmodulin. *Circ. Res.* **90**, E49–E57 (2002).
34. Kim, J. *et al.* Calmodulin mediates Ca^{2+} sensitivity of sodium channels. *J. Biol. Chem.* **279**, 45004–45012 (2004).
35. Mori, M. *et al.* Novel interaction of the voltage-dependent sodium channel (VDSC) with calmodulin: does VDSC acquire calmodulin-mediated Ca^{2+}-sensitivity? *Biochemistry* **39**, 1316–1323 (2000).
36. Clackson, T. & Wells, J.A. A hot spot of binding energy in a hormone-receptor interface. *Science* **267**, 383–386 (1995).
37. Leavitt, S. & Freire, E. Direct measurement of protein binding energetics by isothermal titration calorimetry. *Curr. Opin. Struct. Biol.* **11**, 560–566 (2001).
38. Jencks, W.P. On the attribution of additivity of binding energies. *Proc. Natl. Acad. Sci. USA* **78**, 4046–4050 (1981).
39. Mouton, J., Feltz, A. & Maulet, Y. Interactions of calmodulin with two peptides derived from the c-terminal cytoplasmic domain of the Ca(v)1.2 Ca^{2+} channel provide evidence for a molecular switch involved in Ca^{2+}-induced inactivation. *J. Biol. Chem.* **276**, 22359–22367 (2001).
40. Xiong, L., Kleerekoper, Q.K., He, R., Putkey, J.A. & Hamilton, S.L. Sites on calmodulin that interact with the C-terminal tail of Cav1.2 channel. *J. Biol. Chem.* **280**, 7070–7079 (2005).
41. Hoeflich, K.P. & Ikura, M. Calmodulin in action: diversity in target recognition and activation mechanisms. *Cell* **108**, 739–742 (2002).
42. Van Petegem, F., Clark, K.A., Chatelain, F.C. & Minor, D.L., Jr. Structure of a complex between a voltage-gated calcium channel beta-subunit and an alpha-subunit domain. *Nature* **429**, 671–675 (2004).
43. Kholod, N. & Mustelin, T. Novel vectors for co-expression of two proteins in *E. coli*. *Biotechniques* **31**, 322–323 326–328 (2001).
44. Kapust, R.B. *et al.* Tobacco etch virus protease: mechanism of autolysis and rational design of stable mutants with wild-type catalytic proficiency. *Protein Eng.* **14**, 993–1000 (2001).
45. Van Duyne, G.D., Standaert, R.F., Karplus, P.A., Schreiber, S.L. & Clardy, J. Atomic structures of the human immunophilin FKBP-12 complexes with FK506 and rapamycin. *J. Mol. Biol.* **229**, 105–124 (1993).
46. McPherson, A. *Crystallization of Biological Macromolecules* (Cold Spring Harbor Press, Cold Spring Harbor, New York, USA, 1999).
47. Otwinowski, Z. & Minor, W. Processing of X-ray diffraction data collected in oscillation mode. *Methods Enzymol.* **276**, 307–326 (1997).
48. Schneider, T.R. & Sheldrick, G.M. Substructure solution with SHELXD. *Acta Crystallogr. D Biol. Crystallogr.* **58**, 1772–1779 (2002).
49. d Fortelle, E.I. & Bricogne, G. Maximum-likelihood heavy atom parameter refinement for multiple isomorphous replacement and multiwavelength anomalous diffraction methods. *Methods Enzymol.* **276**, 472–494 (1997).
50. Terwilliger, T.C. Maximum-likelihood density modification. *Acta Crystallogr. D Biol. Crystallogr.* **56**, 965–972 (2000).
51. Perrakis, A., Morris, R. & Lamzin, V.S. Automated protein model building combined with iterative structure refinement. *Nat. Struct. Biol.* **6**, 458–463 (1999).
52. McRee, D.E. XtalView/Xfit–A versatile program for manipulating atomic coordinates and electron density. *J. Struct. Biol.* **125**, 156–165 (1999).
53. Collaborative Computational Project, Number 4. The CCP4 suite: Programs for protein crystallography. *Acta Crystallogr. D Biol. Crystallogr.* **50**, 760–763 (1994).
54. Edelhoch, H. Spectroscopic determination of tryptophan and tyrosine in proteins. *Biochemistry* **6**, 1948–1954 (1967).